



HAL
open science

Modelling of the coupling hydrodynamic transfer for a gas-liquid countercurrent flow on a wavy surface

Stéphane Negny, Michel Meyer, Michel Prevost

► **To cite this version:**

Stéphane Negny, Michel Meyer, Michel Prevost. Modelling of the coupling hydrodynamic transfer for a gas-liquid countercurrent flow on a wavy surface. *Chemical Engineering Science*, 2003, 58 (12), pp.2705-2714. 10.1016/S0009-2509(03)00123-4. hal-03603056

HAL Id: hal-03603056

<https://hal.science/hal-03603056>

Submitted on 9 Mar 2022

HAL is a multi-disciplinary open access archive for the deposit and dissemination of scientific research documents, whether they are published or not. The documents may come from teaching and research institutions in France or abroad, or from public or private research centers.

L'archive ouverte pluridisciplinaire **HAL**, est destinée au dépôt et à la diffusion de documents scientifiques de niveau recherche, publiés ou non, émanant des établissements d'enseignement et de recherche français ou étrangers, des laboratoires publics ou privés.

Modelling of the coupling hydrodynamic transfer for a gas–liquid countercurrent flow on a wavy surface

S. Negny, M. Meyer*, M. Prévost

INP-ENSIACET/CNRS UMR 5503, Groupe Séparation Gaz-Liquide, 118 Route de Narbonne, 31077 Toulouse Cedex 04, France

Abstract

This paper concerns laminar countercurrent gas–liquid flow over a wavy wall column, in the case of a falling liquid film. The modelling concerns the coupling of hydrodynamic and heat and mass transfer for an absorption as an example of application. The falling liquid film interacts, through the free interface, with the gas phase. The wavy surface generates particular hydrodynamic conditions with the presence of a vortex in both phases. The consequence of these vortices is an increase of transfers compared to the smooth wall.

Keywords: Falling film; Wavy surface; Coupling hydrodynamic transfer; Gas–liquid flow; Free interface; Vortex

1. Introduction

The gas–liquid contactors are one of the most wide-spread chemical engineering apparatus. The flow of liquids in falling thin films with a countercurrent of vapour is widely encountered in many industrial applications such as stream condensers, evaporators, wetted wall columns, absorbers in heat pumps and gas treatment, reactors, etc. These kind of gas–liquid contactors do not escape to one of the current orientation in chemical engineering: increasing transfer without enhancing apparatus size. The fluxes of heat and mass transfer, in both liquid and gas phases, are usually related to the flow pattern. Therefore, many investigations are carried out to search for new wall designs, to obtain hydrodynamical conditions which enhance transfer. These new wall designs, corrugated surfaces, consist of a deformation of the solid wall shape. There are numerous types of corrugated surfaces, refer to the work done by Miller and Perez Blanco (1993) for details, for few of them. The wavy surface is one of the corrugated surfaces which offers a greater liquid film stability.

Firstly the wavy surfaces are used in full duct, such as in: compact heat exchangers to enhance heat transfer and in blood oxygenator to increase mass transfer. Thus, numerical and experimental studies on channels with wavy

walls arise to investigate the above applications. Nishimura, Ohory, Kajimoto, and Kawamura (1984, 1985), Nishimura, Ohory, Tarumoto, and Kawamura (1986) and Nishimura, Murakami, Arakawa, and Kawamura (1990) have published several reports on the flow pattern and transfer fluxes. Their research widely cover laminar, transitional and turbulent regimes. In a laminar flow regime ($Re < 350$), the results showed a two-dimensional steady vortex in the furrows. The presence of the vortex enhances of the transfer through the wall compared to the smooth wall, under the same inlet flow conditions. It is for these particular hydrodynamic conditions and their resulting transfer performances that we decide to use wavy surface for a film flow. The flow of film over wavy surface is a new type of contactor, so the available literature on this domain is limited.

The increased usage of powerful computers enables more and more detailed and precise models to be solved. The initial heat and mass transfer models were based on a theoretical stage approach. They were improved by indirectly introducing hydrodynamics via transfer coefficients. Currently, the models are refined towards a local approach by directly introducing hydrodynamic patterns, which determine simultaneous transfer. This procedure avoids the usage of heat and mass transfer coefficients. In this paper, this approach is applied to the case of absorption of sulphur dioxide (SO_2)-air mixture with air by a falling film of tetraethylen glycol dimethyl ether (E181). These non-conventional constituents are selected to meet an industrial requirement; the

* Corresponding author.

E-mail address: michel.meyer@ensiacet.fr (M. Meyer).

treatment of atmospheric rejects. The E181 was chosen because of its high solubility with respect to SO_2 (Sciamanna & Lynn, 1988).

The first part of this paper is dedicated to the modelling stage. As well as the numerical method, this part deals also with the difficulties associated with resolution, caused by the wall design. In the second part, the simulation results based on a local approach of all transfer phenomena are presented. In order to quantify the efficiency of the wavy wall, the results are compared with these of the smooth wall.

2. Details of the numerical simulation

2.1. A problem description

The physical problem numerically simulated here, is the flow, heat and mass transfer for two fluids with countercurrent flows. The system is composed of a falling liquid film interacting across the interface with a gas flow. The falling liquid film flows over a new type of column wall, i.e., a wavy surface. The wavy surface is a specific example, the presented model and resolution method can be extended to other surface designs, only if the surface geometry does not have horizontal tangent.

As the surface shape is periodical and the flow readily established, the modelling is reduced for one furrow. Fig. 1 presents the problem geometry and the different geometrical parameters. The wall is assumed to be sinusoidal, consequently its shape is given by the following equation:

$$r_p = r_m + a \cos\left(\frac{2\pi z}{p}\right). \quad (1)$$

The reciprocal action between both phases is taken into account at the interface. Consequently, it is necessary to know the interface position. One of the main characteristics of our model is that the interface is completely free, and able to move, i.e. the interfacial radius is a variable of the system.

Section 2.2 presents the governing equations for hydrodynamics, heat and mass transfer for both phases. Section 2.3 explains the boundary conditions. The reciprocal interactions of the two phases (for hydrodynamics and heat and mass transfer), are taken into account through the interfacial boundary conditions. The numerical treatment method for these interactions is detailed in Section 2.4.

2.2. Modelling

Firstly we shift our attention to the hydrodynamics model. A brief presentation is given, summing up the principal assumptions and equations of the two phases. A more detailed approach has been published previously, but only for the liquid phase (the gas phase is assumed to be stagnant) (Negny, Meyer, & Prévost, 2001a). Here, the previous model is extended to include the gas phase. The problem investigated

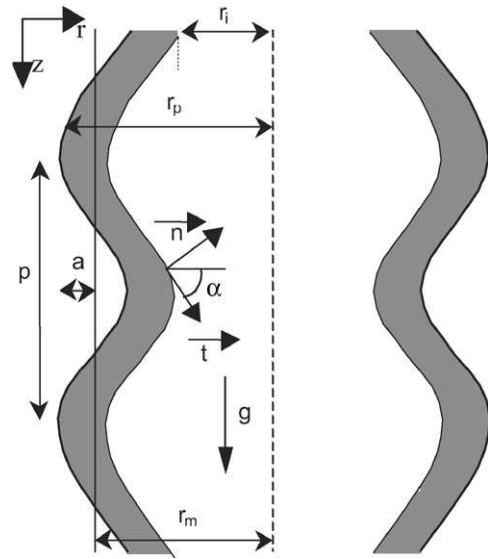


Fig. 1. Geometrical description of one furrow.

is Newtonian and incompressible fluids under a laminar flow regime, with all fluid properties constant. The Navier–Stokes equations are formulated in terms of stream function and vorticity for both phases.

Concerning this subject, another way to proceed is to use the projection method applied by De Angelis, Lombardi, and Banerjee (1997) who worked with the primitive variables (velocity/pressure). This method requires boundary conditions for pressure, and more specifically, in the normal direction of the interface. As previous authors have mentioned in their paper, the widely used boundary condition ($\partial P/\partial n = 0$) leads to a decrease in accuracy, close to the boundaries. In the case of a very thin film of liquid, the error generated by this boundary condition will be penalising. Moreover, the main goal of this study is to quantify the benefits of the wavy wall on the transfers. This benefit effect is a consequence of the hydrodynamics engendered by the wall shape. To achieve this goal, a new approach is used which directly introduces the hydrodynamics condition in the transfer equation. Consequently, the pressure field is not a main variable of interest in our case. Finally, to avoid the problem of pressure boundary condition, the vorticity and stream function formulation for the Navier–Stokes equations is chosen.

One more equation is needed to determine the interface position, because it is assumed to be free (the variable r_i is added, therefore one more equation is necessary). This interface position is reached through employing a specific equation, which is based on a force balance and makes the following assumptions: there are no ripples and there is constant surface tension. An additional assumption of this equation is that the gas phase is stagnant, without making this assumption, the problem is too complex and the equation is able to be solved. Further details on the demonstration, which leads to this equation are given by Slattery (1990) and Negny (1999). After an experimental validation of the

interface position and profile given by this equation, by an optical method (Negny, Meyer, & Prévost, 2001b) in the case of a stagnant phase, it is applied to a moving gas phase under the same formulation. This paper considers a flowing gas stream regime, but under laminar flow regime the assumption of stagnant gas phase still holds and does not result in a significant error (as shown in the results section). The theoretical investigation leads to the following system:

$$-\frac{1}{r} \frac{\partial(\psi^l, \omega^l)}{\partial(r, z)} - \frac{1}{r^2} \frac{\partial\psi^l}{\partial z} \omega^l = v^l \nabla^2 \omega^l,$$

$$\omega^l = \nabla^2 \psi^l,$$

$$r_i^2 \left(\frac{d^3 r_i}{dz^3} - \frac{1}{\sigma} \frac{\partial P}{\partial z} \right) + \frac{dr_i}{dz} = 0, \quad (2)$$

$$-\frac{1}{r} \frac{\partial(\psi^g, \omega^g)}{\partial(r, z)} - \frac{1}{r^2} \frac{\partial\psi^g}{\partial z} \omega^g = v^g \nabla^2 \omega^g,$$

$$\omega^g = \nabla^2 \psi^g. \quad (3)$$

The equations relating to the model, which is dedicated to the simultaneous heat and mass transfer for a multicomponent mixture, are written in terms of fluxes. The transfer fluxes are composed of two terms: conduction and convection. The conduction fluxes are respectively evaluated by the Fick's law for mass transfer and Fourier's law for heat transfer. It can be noticed, that for the former Maxwell Stephan's law can also be applied. Hydrodynamic conditions are directly introduced in the convection fluxes through the velocity field. The axial diffusion is neglected with respect to the convection, for the mass transfer and, similarly, the axial heat conduction is neglected in the case of heat transfer. In order to have the same number of equations and unknowns, two more equations are necessary. These equations are based on two classical rate balance equations. The model is written for each phase, with the introduction of the velocity field, the diffusion coefficient and the thermal conduction coefficient of the corresponding phase. Thus, the complete heat and mass transfer model is as follows:

$$N_r^{lj} = v_r^l C^{lj} - D_{jm} \frac{\partial C^{lj}}{\partial r},$$

$$N_z^{lj} = v_z^l C^{lj},$$

$$q_r^l = -\lambda^l \frac{\partial T^l}{\partial r} + \sum_j N_r^{lj} \bar{H}^{lj},$$

$$q_z^l = \sum_j N_z^{lj} \bar{H}^{lj},$$

$$\frac{\partial N_z^{lj}}{\partial z} + \frac{\partial N_r^{lj}}{\partial r} + \frac{1}{r} N_r^{lj} = 0,$$

$$\frac{\partial q_z^l}{\partial z} + \frac{\partial q_r^l}{\partial r} + \frac{1}{r} q_r^l = 0, \quad (4)$$

$$N_r^{gj} = v_r^g C^{gj} - D_{jm} \frac{\partial C^{gj}}{\partial r},$$

$$N_z^{gj} = v_z^g C^{gj},$$

$$q_r^g = -\lambda^g \frac{\partial T^g}{\partial r} + \sum_j N_r^{gj} \bar{H}^{gj},$$

$$q_z^g = \sum_j N_z^{gj} \bar{H}^{gj},$$

$$\frac{\partial N_z^{gj}}{\partial z} + \frac{\partial N_r^{gj}}{\partial r} + \frac{1}{r} N_r^{gj} = 0,$$

$$\frac{\partial q_z^g}{\partial z} + \frac{\partial q_r^g}{\partial r} + \frac{1}{r} q_r^g = 0. \quad (5)$$

It is important to emphasise that this model is very global. It can be applied to every kind of unit operations provided that the corresponding velocity field is introduced and the right boundary conditions are specified.

2.3. Boundary conditions

The boundary conditions characterise the specified unit operation that is going to be solved (and they define the solution of the problem). Firstly, the hydrodynamic boundary conditions are addressed, and secondly, the heat and mass transfer conditions are presented.

2.3.1. Hydrodynamics boundary conditions

All of the boundary conditions are expressed in terms of velocity to give a greater understanding, however in agreement with Eqs. (2) and (3) they are translated in stream function and vorticity for the resolution. The wall shape design inspires periodical conditions for the velocity at the inlet and outlet of the furrow (as the wall is assumed to be sinusoidal). In the laminar flow regime this assumption was experimentally corroborated in the case of a stagnant gas phase. We can assume that it can be applied to this case:

$$v^l(z=0) = v^l(z=p) \quad (6)$$

$$v^g(z=0) = v^g(z=p). \quad (7)$$

At the wall, no slip conditions are used between the liquid and the solid surface:

$$v^l = 0(r=r_p). \quad (8)$$

The fluids flow inside a circular tube, so there is an axisymmetric problem. Consequently, symmetrical conditions can be applied at the centre of the tube for the gas phase

$$\left. \frac{\partial v^g}{\partial r} \right|_{r=0} = 0. \quad (9)$$

Now the conditions at the interface are expressed. The velocity, normal to the stationary interface is zero for each

phase:

$$v^l \cdot n = v^g \cdot n = 0, \quad (10)$$

where n and t are unit vectors, respectively, locally, normal and tangential to the interface, shown in Fig. 1. The unit vectors are determined by the following expressions:

$$t = \frac{1}{\sqrt{1 + \frac{dr_i}{dz}^2}} \begin{pmatrix} 1 & dr_i/dz \\ dr_i/dz & -1 \end{pmatrix}. \quad (11)$$

Furthermore, the continuity of the tangential velocity across the interface gives the following expression:

$$v^l \cdot t = v^g \cdot t. \quad (12)$$

Shear and normal stresses balance on the interface, complete the boundary conditions:

$$(\tau^l \times n)t = (\tau^g \times n)t \quad (13)$$

$$(\tau^l \times n)n - (\tau^g \times n)n = \sigma \frac{dr_i/dz}{\sqrt{1 + \frac{dr_i}{dz}^2}}. \quad (14)$$

Now that the hydrodynamic model is complete, the heat and mass transfer boundary conditions are addressed.

2.3.2. Heat and mass transfer boundary conditions

As mentioned previously, the boundary conditions define the problem. Here, it is the absorption of SO_2 by a falling film of E181. At the entrance, the temperature and the concentration of all species in both fluids are known. Furthermore, the velocity fields and results of the hydrodynamic model, are given. Therefore, the axial heat and mass transfer fluxes are able to be determined.

$$\text{For the liquid } z = 0: \quad N_z^{jl} = v_z^l C^{j0} = N_z^{j0}, \quad (15)$$

$$q_z^l = \sum_j N_z^{j0} H^{j0} = q_z^{l0}. \quad (16)$$

$$\text{For the gas } z = p: \quad N_z^{jg} = v_z^g C^{j0} = N_z^{jg0}, \quad (17)$$

$$q_z^g = \sum_j N_z^{jg0} H^{j0} = q_z^{g0}. \quad (18)$$

For the liquid, the temperature at the wall is kept constant throughout all the simulations. The wall is a none porous solid surface, hence no mass is transferred through it.

$$\text{At } r = r_p: \quad T^l = T_p \quad (19)$$

and

$$N_r^{jl} = 0. \quad (20)$$

For the gas phase, at the centre, the concentrations and temperature are symmetrical with respect to the furrow

geometry.

$$\text{At } r = 0: \quad \frac{\partial T^g}{\partial r} = 0 \quad (21)$$

and

$$\frac{\partial C^{jg}}{\partial r} = 0. \quad (22)$$

For the interface, equilibrium is reached and there is continuity of temperature, heat and mass transfer fluxes. Once again, the interactions between the two phases are taken into account at the interface.

$$\text{At } r = r_i: \quad C^{lj} = C_{eq}^{lj}, \quad (23)$$

$$T^g = T^l, \quad (24)$$

$$N_r^{jg} = N_r^{jl}, \quad (25)$$

$$q_r^l = q_r^g. \quad (26)$$

2.3.3. Coupling of the two phases

This part concerns the chosen method employed to solve the model. At this point there is one model decomposed from the hydrodynamics, heat and mass transfer equations with the associated boundary conditions. As mentioned previously, one of our objectives is to present a model which is characterised by the coupling between a detailed description of the hydrodynamics and the simultaneous heat and mass transfer in order to study the narrow link between both parts. Even now, it is difficult to simultaneously solve the motion, heat and mass transfer equations. This difficulty is addressed by decomposing the model into two separate models, using a sequential approach: the first part is the hydrodynamics, with two fluids moving in opposite directions, and the second part is the heat and mass transfer. The velocity field links the two parts, i.e. it is the result of the first part and it is included into the second one in order to evaluate transfer rates. This decomposition assumes that heat and mass transfer do not influence hydrodynamics. The model is applied to one furrow, which is 25×10^{-3} m long (Section 3), consequently on this short length the intensity of transfers is not important enough to disrupt hydrodynamics.

Up to this point, we have seen that the problem is decomposed into two models: hydrodynamics and heat and mass transfer. In each model, the two phases can be entirely solved directly, but the solution will require the inversion of very large matrices (see numerical resolution) and it will be very expensive in terms of computational resources requirements. Meanwhile, in order to fully satisfy the interfacial conditions for each model, an iterative method is set up: resolution of the liquid phase followed by the resolution of the gas phase. For each model, four interfacial boundary conditions are specified. For this iterative procedure, these

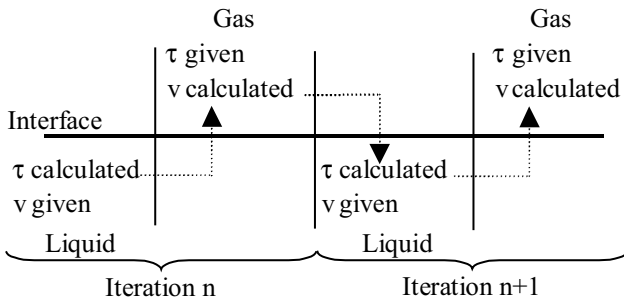


Fig. 2. Gas–liquid coupling at the interface.

interfacial conditions are separated: two by phase. The iterations are stopped when the four conditions are satisfied simultaneously. For example, for the hydrodynamics model, the iterative procedure can be realised by using the velocity field for boundary conditions and calculating the shear stress field at the interface for one phase. For the other phase, the shear stress field is set and the velocity field is calculated. This procedure is iterated while the velocity and shear stress fields are not satisfied simultaneously at the interface at the same iteration. In fact, the iterative procedure is a method of successive substitutions. It is noticed that the iterative method is just a numerical trick with no more assumptions. For the same calculation power, the iterative method allows the use of a more refined grid.

Nevertheless, in chemical engineering operation, it is the gas that imposes a shear stress on the liquid. Consequently, the boundary conditions are implemented with the shear stress continuity on the liquid phase (i.e. shear stress known at the interface) and the velocity boundary conditions for the gas phase, as it is suggested by Lombardi, De Angelis, and Banerjee (1996). This procedure is summarised in Fig. 2. For the heat and mass transfer model, the same method of successive substitutions is used. In short, the initial model is decomposed in four blocs:

Hydrodynamics model

1st bloc liquid phase: Eq. (2) boundary conditions no. 6, 8, 13, 14

2nd bloc gas phase: Eq. (3) boundary conditions no. 7, 9, 10, 12

Heat and mass transfer model

3rd bloc liquid phase: Eq. (4) boundary conditions no. 15, 16, 19, 20, 23, 26

4th bloc gas phase: Eq. (5) boundary conditions no. 17, 18, 21, 22, 24, 25

It is evident that the liquid model is composed of Eqs. (2) whereas the gas phase model is limited to Eqs. (3). This is because the interface position is determined by the liquid model. For both models (hydrodynamics, heat and mass

transfer), the method of successive substitutions is assumed to reach the part of converged when the four interfacial boundary conditions are satisfied simultaneously at the same iteration:

For hydrodynamics: Convergence criterion 1: 10, 12, 13, 14 satisfied

For heat and mass transfer: Convergence criterion 2: 23, 24, 25, 26 satisfied

2.3.4. Resolution

This part is the last stage of the solution to this problem. After separating the hydrodynamics and transfer part, and then the gas and liquid phase, the resolution method for each phase of each part is presented. Here, only a summary of the method is presented, to have more details see Negny et al. (2001a). The wall shape design increases the complexity of the calculation domain, and thus does not allow the classical finite differences scheme to be used. Furthermore, the interface is free, the film thickness is able to axially move which leads to possible irregularity in axial discretisation. In order to transform the physical domain into a mathematical one, which contains rectangular co-ordinates, an algebraic transformation, suggested by Panday (1990) is extended to our problem. The two phases are solved separately, therefore, there is a transformation by phases in the radial direction:

$$\eta^l = \frac{r - r_i}{r_p - r_i} \text{ (liquid)}, \quad \eta^g = \frac{r}{r_i} \text{ (gas)},$$

$$\xi = z \text{ (gas and liquid)}.$$

For both models and both phases, the various equations and boundary conditions are transformed and discretised in this new mathematical domain. For all systems, the discretisation step leads to systems of non-linear algebraic equations, solved by an iterative Newton–Raphson method. For the resolution, the Jacobian matrices are analytically evaluated and a judicious arrangement gives sparse matrices. In order to reduce the CPU time, these particular matrices structures are exploited in the resolution. The principal inconvenience of the Newton–Raphson method is that it is locally convergent, initialisation is therefore an important point. Thus, for a fixed Reynolds number, the results of the smooth tube initialise the simulation and the wave amplitude is gradually increased until its final value, i.e. is used as a homotopic parameter. Each time, the initialisation is performed with the results of the preceding wave amplitude. This way of initialisation is inspired from the continuation and homotopic method which are global method.

All different levels of the resolution are clearly summed up in Fig. 3: the two models, the successive substitutions and the Newton–Raphson method.

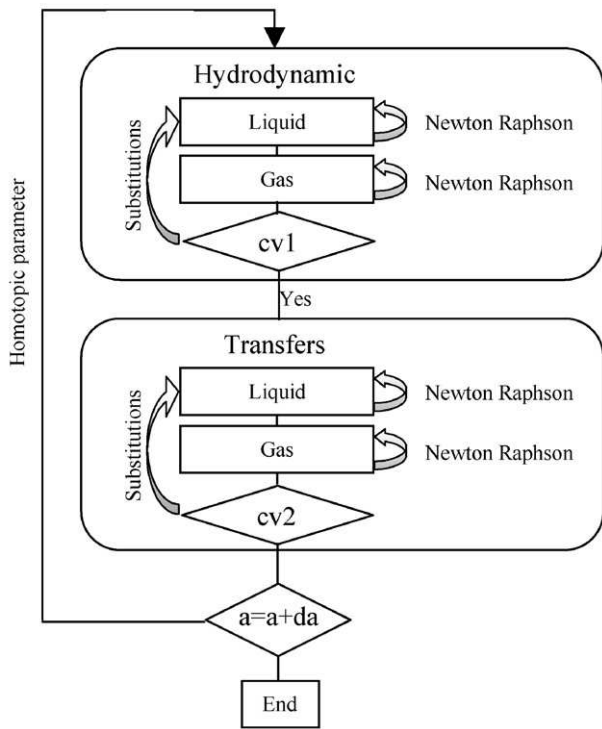


Fig. 3. Resolution scheme.

3. Results

As it was explained previously, the results are presented for the absorption of SO_2 gas by a falling film of E181. For reasons, other than the industrial requirement for this choice, are that the mixture is in agreement with the heat and mass transfer assumptions: absorption without chemical reaction and non-volatile solvent. At atmospheric pressure, the boiling point of E181 is 548 K.

The geometric characteristics of the furrow are: $a = 5 \times 10^{-3}$ m, $p = 25 \times 10^{-3}$ m and $r_m = 45 \times 10^{-3}$ m. In order to quantify the efficiency of the wavy wall, the results are compared with those of the smooth wall, with a radius equal to the average radius of the wavy surface. At the entrance, the liquid phase is pure E181 at atmospheric pressure and at a temperature of 293 K. For the gas phase, a mixture of air and SO_2 (0.15 molar fraction) enters under the same conditions.

3.1. Hydrodynamic results

Before to simulate our operation, the model was tested for a particular case: a falling film flowing inside a smooth wall with a countercurrent of gas. Using the same assumption of no ripples on the interface, and keeping the boundary conditions constant, an analytical solution of the velocity field of both phases and of the film thickness can be reached. The film thickness is not analytically calculated by the interface equation, but by another equation based on the flow

rate and mean velocity. The calculated film thickness differs by around 4% from the analytical results. Concerning the velocity field, the error is in the same order of magnitude. It is important to notice that the difference between the calculated thickness and the analytical thickness is only 0.5% when the gas phase is stagnant. The difference is more significant in the case where the gas is calculated, because the assumption of the interfacial equation does not take circulating gas into account. Nevertheless, a difference of 4% is weak for the present problem. Even if the interfacial equation is established with a restrictive assumption, it describes correctly the problem.

As specified previously in Section 2.2 an experimental validation of the hydrodynamics was set up for the case of a stagnant gas phase (Negny et al., 2001b). It consists of the determination of the interface position and profile by an optical method. With the validation of the interface position (i.e. film thickness), we validate the velocity field, because the film is very thin. Consequently, a difference between the experimental and the calculated velocity field will result in a deviation between both thicknesses. The ratio between the calculated and experimental thickness is presented in Figs. 4(a) and (b). An agreement between both thicknesses can be reached. Therefore, the model is validated in the case of a stagnant gas phase. In the model presented in this paper, the gas is flowing in laminar flow range, consequently, its influence on the interface position is not significant. This is clearly demonstrated in the previous analytical validation for the falling film flowing over a smooth wall. With this experimental validation and with the small deviation introduced by the circulation of gas, the exploitation of the model in the case of gas circulation is assumed to be reliable.

The flow pattern is exposed in terms of calculated streamlines, Figs. 5(a)–(c): the continuous streamlines for the liquid and the dashed lines for the gas. We can see for the liquid that during the laminar regime, the particular wall design drives the appearance of a vortex in the second part of the furrow, near the wall. This vortex arises for a liquid with a Reynolds number of 15. The more the Reynolds number increases for the liquid, the more the vortex size and strength of recirculation are enhanced.

Now, we try to explain the vortex formation in the liquid phase. The influence of the viscosity is situated in the thin boundary layer near the solid wall. For the flow outside this boundary layer (where the friction is weak), the fluid particles are accelerated from A to B and decelerated on the second part of the furrow (B to C). Hence, the pressure decreases from A to B and increases from B to C. The particles inside the boundary layer are in the same pressure field. These particles lose a great part of their kinetic energy to counter the friction forces on the first part of the furrow (A to B). At B, their kinetic energy is not strong enough to win the pressure gradient between B and C. As a consequence, they cannot reach C, the pressure gradient imposes a change of flow direction and the vortex arises near the wall. Two particular points emerge from the above

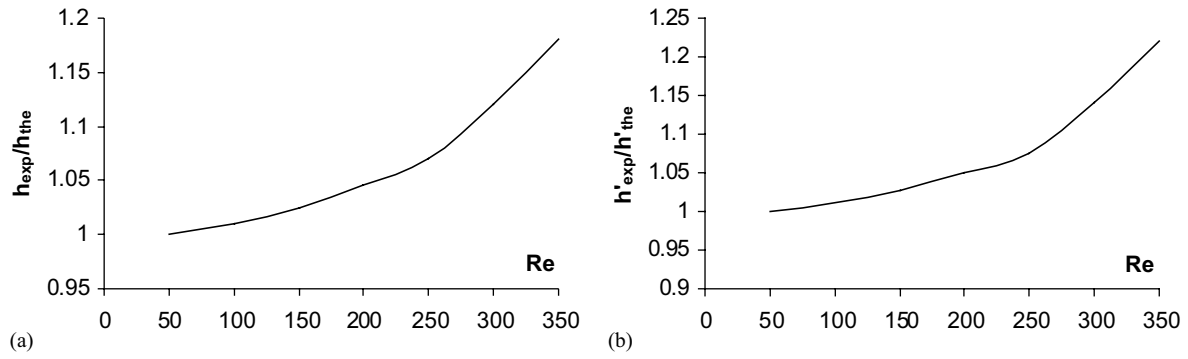


Fig. 4. Comparison between the calculated and experimental film thickness: (a) Ratio of mean thickness (region without recirculation) and (b) Ratio of the maximum mean thickness.

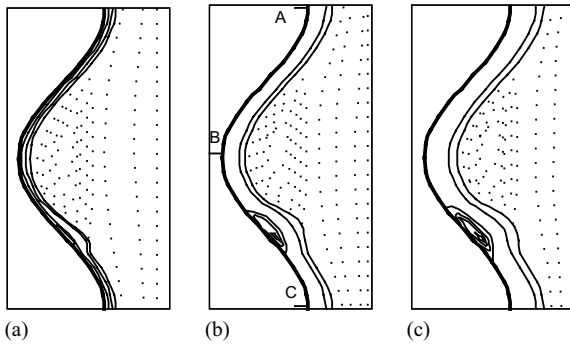


Fig. 5. Streamlines for $Re_g = 300$ and various Re_l : (a) $Re_l = 15$, (b) $Re_l = 150$ and (c) $Re_l = 300$.

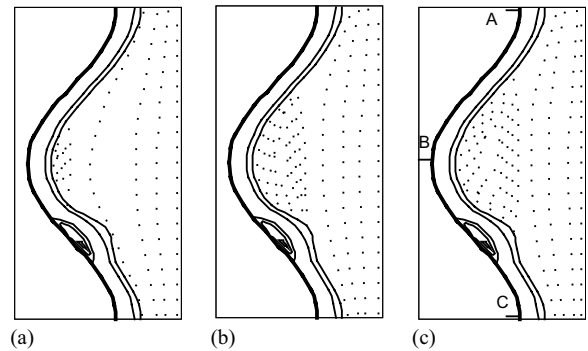


Fig. 6. Streamlines for $Re_l = 150$ and various Re_g : (a) $Re_g = 15$, (b) $Re_g = 150$ and (c) $Re_g = 300$.

explanation. The separation point is where the flow begins to leave the wall and the reattachment point where the flow reattaches to the wall.

The film thickness is also affected by the vortex. On the first part of the furrow, the film thickness remains constant until the vortex. At this location the film becomes thicker and reaches its maximum thickness value at the vortex centre. Afterwards, the film thickness returns to its initial value. When the liquid Reynolds number increases, the film thickness is enhanced because of the vortex growth, and the vortex centre shifts downstream. This behaviour is encountered all along the laminar regime. Experimentally, the laminar regime is kept until $Re = 300$, hereafter the flow becomes turbulent with an unsteady motion for the vortex.

Concerning the gas, here again there is the formation of a vortex in the trough of the furrow, Fig. 6(a)–(c). The vortex formation can be explained in the same manner as that of the liquid case. The only difference is that at the interface, the gas is in motion, whereas the velocity of the liquid at the wall is zero. For a fixed liquid Reynolds number, when the gas Reynolds number increases, the gas vortex size and strength are enhanced. In the case of the flow of one fluid in a full duct, the separation point is moved downstream and the reattachment point is moved upstream for increasing Reynolds number. Here, it is the same, but in a less im-

portant manner, for the liquid reattachment and separation points for a flow of film. For the gas points, we can emphasise that the points start to evolve in the same way. However for a Reynolds number of 100, the gas separation point stays at the same location which corresponds to the maximum film thickness (centre of the liquid vortex). For this gas Reynolds number, the location of the separation point is further upstream compared to its location in a full duct. Therefore, the liquid vortex behaves like an obstacle and promotes the separation of the gas flow.

The focus is now moved to the influence of the liquid flow for a fixed gas Reynolds number. The evolution of the gas vortex is very weak because the film thickness is not very important. The more the liquid Reynolds number increases, the thicker the film becomes. As a consequence, the gas vortex size decreases. In fact, for a gas Reynolds number greater than 100, the gas reattachment point shifts downstream. For a gas Reynolds number smaller than 100, the gas separation point moves upstream and the reattachment point downstream. These evolutions are almost imperceptible due to the thin film thickness.

3.2. Heat and mass transfer results

In order to compare the performance of the wavy wall with regard to the smooth one, the results are presented in terms

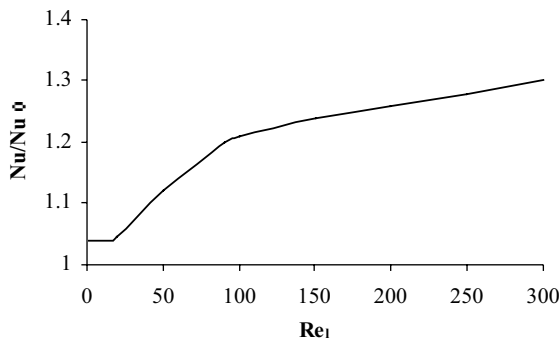


Fig. 7. Ratio of global wall Nusselt numbers.

of global Nusselt number (on one furrow) for heat transfer through the wall, and with the global Sherwood number for mass transfer at the interface. To estimate these numbers, we need transfer coefficients. As it has been shown before, the hydrodynamic is directly introduced in the transfer, thus transfer coefficients are avoided, however it is the software package that calculates these transfer coefficients so that a comparison can be made between both wall designs. The calculations of these coefficients, the Nusselt and Sherwood numbers are explained in a previous paper (Negny et al., 2001a).

First, the evolution of the Nusselt number along the laminar flow regime for a gas Reynolds number of 300 is examined in Fig. 7. The principal comment is that the ratio increases during the laminar flow regime. More precisely, in this figure three zones are distinguished. The first zone is for a liquid Reynolds number between 1 and 15, the ratio is constant until the formation of the vortex, because the velocity fields are semi-parabolic in both cases. Nevertheless, the ratio is greater than one because of the increase of transfer area for the same column length on behalf of the wavy surface. The second zone is for a liquid Reynolds number between 15 and 100, and the third is defined for a liquid Reynolds number between 100 and 300 (end of the laminar regime). The increasing trend is located in both zones and it can be decomposed in two parts which corresponds to the vortex intensification steps. Indeed, with the reverse flow, the vortex cuts off the thermal boundary layer and it is renewed with fresh liquid from the main stream. The more the vortex is intensified, the more the thermal boundary layer is renewed, and the more the heat transfer increases. A local analysis of heat transfer and local Nusselt number, shows that the Nusselt number increases at the vortex location and reaches its maximum value at the reattachment point, where the particular flow enhances heat transfer.

The ratio between the Sherwood numbers is plotted in Fig. 8 for a liquid Reynolds number of 150. As for the Nusselt numbers, the curve can be decomposed into three zones. The first corresponds to a constant ratio until the gas Reynolds number is equal to 15, due to same hydrodynamic conditions in both cases. When the vortex arises the ratio

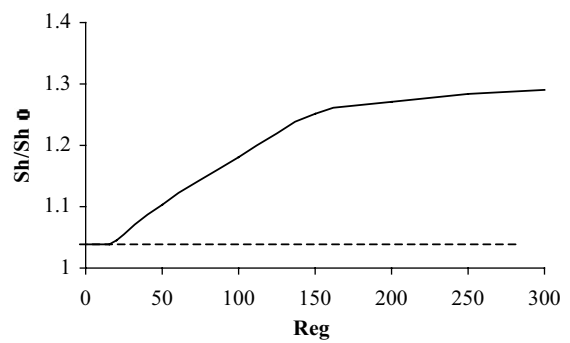


Fig. 8. Ratio of global interfacial Sherwood numbers.

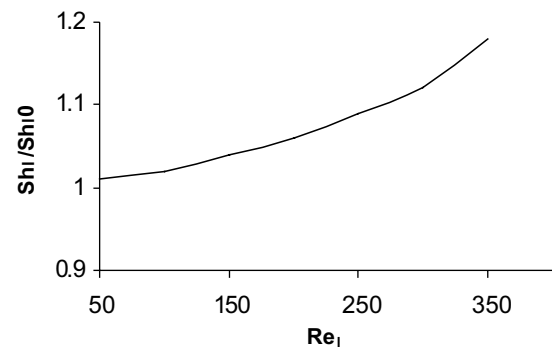


Fig. 9. Ratio of local liquid Sherwood numbers.

starts to increase. It increases all along the laminar flow regime because the vortex recirculates with more strength. In the second zone, the enhancement is more significant because the intensification of the vortex is important. In the third zone, the vortex recirculation increases less significantly, and as a consequence the ratio does the same. To gain a better understanding of the phenomenon, the global Sherwood number is decomposed into two parts: the gas Sherwood number and the liquid Sherwood number. The liquid Sherwood number has a weak enhancement in the end of the laminar regime, Fig. 9. In fact, in this phase the recirculation zone is not wide enough to reach the interface. Hence, the concentration boundary layer is not affected and renewed by the vortex. Therefore, the characteristics of mass transfer are the same as the case of the smooth surface. Nevertheless, there is a slight increase when the liquid Reynolds number is enhanced. Much of the increase is caused by heat transfer enhancement. It is confirmed by simulations with mass transfer alone, the liquid Sherwood number has a less of an increase than in the simultaneous heat and mass transfers.

In Fig. 8, the dashed line represents the global Sherwood number with a stagnant gas (without gas flow). The gap between the two curves represents the influence of the gas phase hydrodynamic conditions on transfer. The benefit effects of the gas flow on the mass transfer start to become significant when the vortex arises and is kept until $Re_g = 150$. After this value, the effect of the gas flow on mass transfer

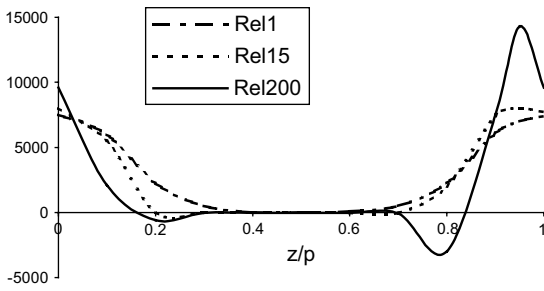


Fig. 10. Non-dimensional wall shear stress.

is limited, because there is a resistance in the liquid which will be explained later.

The gas side local Sherwood number is responsible for the increase of global Sherwood number. In this phase, the vortex is situated near the interface. The gas concentration boundary layer can profit by the renewal caused by the vortex as explained before. As a consequence, in this example, the limiting step of interfacial mass transfer is the liquid side resistance, in Fig. 8, after $Re_g = 150$, the global Sherwood number is fairly constant, which proves that the resistance is in the liquid phase.

To refine this analysis, the heat transfer at the wall and the mass transfer at the interface are studied all along one furrow. To gain a better understanding, attention is focused on the wall shear stress and the interfacial shear stress along the furrow. In both cases, when the vortex appears, the stresses become negative between the separation and the reattachment points for the wall shear stress, Fig. 10. The interfacial shear stress follows a similar curve. The curves have two minimum located at the separation and reattachment points. The minimum at the reattachment point is more pronounced and it is followed by a maximum. In both phases, the separation and reattachment points display a particular local flow with a more important stress (analogous results were found by Sobey (1980) in the case of a full duct).

Returning to the transfer part, the distribution of the wall Nusselt number along the furrow shows an increase at the vortex location and reaches its maximum value at the reattachment point where the wall shear stress becomes significant. At this point, the particular flow put in highlighted, is of benefit to heat transfer. The same explanation can be done for mass transfer at the interface under the same hydrodynamics condition: reverse flow and particular flow at the reattachment point. In both cases, when the Reynolds number is enhanced, the different phenomenon previously presented are always visible, but in a more pronounced way.

4. Conclusion

A numerical model for the simulation of coupling of hydrodynamic and heat and mass transfer for a film, flowing

over a wavy surface, interacting with a countercurrent of gas, has been presented. The model is stated for two Newtonian, incompressible fluids flowing in the laminar regime. The coupling is realised by a sequential approach. Firstly, the hydrodynamics model is presented. The resolution gives the velocity fields, which is directly introduced in the heat and mass transfer model, in terms of transport.

It has been shown that this wall design generates particular hydrodynamic conditions, which are able to enhance the simultaneous heat and mass transfer. These particular hydrodynamic conditions are two vortices that generate mixing effects, which benefit transfers. The vortices renew the boundary layers with fresh fluid, increasing the exchange. It is evident that in the case of mass transfer through the interface, the contribution of heat transfer and hydrodynamic must be dissociated. In the gas phase, the vortex destroys and renews the boundary layer, decreasing the mass transfer resistance in this side. Meanwhile, in the example treated here, the principal mass transfer resistance is located in the liquid side. It does not benefit directly from the mixing effect because the liquid vortex is not wide enough to reach the interface. Nevertheless, the liquid vortex increases the heat transfer through the wall, because it is located near the solid surface. This increase of heat transfer results in enhanced mass transfer. Finally, the total increase of mass transfer can be decomposed in the following way: 65% is due to hydrodynamic in gas phase and 35% is due to heat transfer.

In conclusion, the wavy wall surface improves transfers compared to the smooth one. These kind of surfaces seem to be useful for operations requiring an important dissipation of heat through the wall, such as evaporation and condensation. These surfaces can improve transfers between phases, especially when the mass transfer resistance is in the gas phase, which is interesting for gas treatment. Another advantage of these surfaces is that for the same capacity of gas treatment, the apparatus size is reduced, which can be useful for heat pumps, for example.

One of our future goals is to extend the model presented above to the turbulent flow range. Difficulties may arise from the free interface because, in the turbulent regime, it is very difficult to model the interface position by an equation. One way to proceed to avoid this inconvenience, is to experimentally determine the interface position and to include it as in the form of data in the model.

Notation

a	wave amplitude, m
C^j	concentration of specie j , mol/m ³
C_{eq}^j	equilibrium concentration, mol/m ³
D_{jm}	diffusion coefficient of specie j in mixture, m ² /s
H^j	partial molar enthalpy of specie j , J/mol
h_{exp}	experimental film thickness, m
h_{the}	calculated film thickness, m

n	normal to the interface
N^j	mass transfer rate of specie j , mol/(m ² s)
Nu	mean Nusselt number for wavy tube
Nu_0	Nusselt number for smooth tube
p	wavelength, m
P	pressure, Pa
q	heat flux, J/(m ² s)
r	radial component, m
r_i	interfacial radius, m
r_m	mean radius, m
r_p	wall radius, m
Re	Reynolds number $Re = 4\Gamma/\mu$
Sh	mean Sherwood number for wavy tube
Sh_l	liquid Sherwood number for wavy tube
Sh_0	liquid Sherwood number for smooth tube
Sh_0	Sherwood number for smooth tube
T	temperature, K
T_p	wall temperature, K
t	tangent to the interface
v	velocity, m/s
z	axial component, m

Greek letters

Γ	mass flow rate divided by the wetted perimeter, kg/(m ² s)
η	radial component in the mathematical domain
λ	heat conduction coefficient, J/(m s K)
μ	viscosity, Pa s
ν	dynamic viscosity
ξ	axial component in the mathematical domain
σ	surface tension, N/m
τ	stress tensor
ψ	stream function
ω	vorticity

Indices and exponents

g	gas phase
l	liquid phase
r	radial component
z	axial component
0	entrance

Mathematical operators

$$\nabla^2 = \frac{\partial^2}{\partial r^2} - \frac{1}{r} \frac{\partial}{\partial r} + \frac{\partial^2}{\partial z^2}$$

References

- De Angelis, V., Lombardi, P., & Banerjee, S. (1997). Direct numerical simulation of turbulent flow over a wavy wall. *Physics of Fluids*, 9, 2429–2442.
- Lombardi, P., De Angelis, V., & Banerjee, S. (1996). Direct numerical simulation of near-interface turbulence in coupled gas–liquid flow. *Physics of Fluids*, 8, 1643–1665.
- Miller, W. A., & Perez Blanco, H. (1993). Vertical-tube aqueous LiBr falling film absorption using advanced surface. AES 31, *International absorption heat pump conferences ASME*. New York: ASME (pp. 185–202).
- Negny, S. (1999). *Modélisation et étude expérimentale d'un film liquide laminaire à interface libre ruisselant sur une surface structurée: Couplage hydrodynamique-transfert de masse et d'énergie*. Thesis INP-ENSIACET, Toulouse, France.
- Negny, S., Meyer, M., & Prévost, M. (2001a). Study of a laminar falling film flowing over a wavy wall column: Part I. Numerical investigation of the flow pattern and the coupled heat and mass transfer. *International Journal of Heat and Mass Transfer*, 44, 2137–2146.
- Negny, S., Meyer, M., & Prévost, M. (2001b). Study of a laminar falling film flowing over a wavy wall column: Part II. Experimental validation of hydrodynamic model. *International Journal of Heat and Mass Transfer*, 44, 2147–2154.
- Nishimura, T., Murakami, S., Arakawa, S., & Kawamura, Y. (1990). Flow observations and mass transfer characteristic in symmetrical wavy walled channels at moderate Reynolds numbers for steady flow. *International Journal of Heat and Mass Transfer*, 33, 835–845.
- Nishimura, T., Ohory, Y., Kajimoto, Y., & Kawamura, Y. (1984). Flow characteristics in a channel with symmetric wavy wall for steady flow. *Journal of Chemical Engineering of Japan*, 17, 466–471.
- Nishimura, T., Ohory, Y., Kajimoto, Y., & Kawamura, Y. (1985). Mass transfer characteristics in a channel with symmetric wavy wall for steady flow. *Journal of Chemical Engineering of Japan*, 18, 550–555.
- Nishimura, T., Ohory, Y., Tarumoto, A., & Kawamura, Y. (1986). Flow structure and mass transfer for a wavy channel in transitional flow regime. *Journal of Chemical Engineering of Japan*, 19, 449–455.
- Panday, P. K. (1990). Laminar film condensation of turbulent vapour flowing inside a vertical tube. *Second international symposium of condensers and condensation*, University of Bath, UK (pp. 473–482).
- Sciamanna, S. F., & Lynn, S. (1988). Solubility of hydrogen sulfide, sulfur dioxide, carbon dioxide, propane, and *n*-butane in poly(glyco ether). *Industrial and Engineering Chemical Research*, 40, 492–504.
- Slattery, J. C. (1990). *Interfacial transport phenomena*. New York: Springer.
- Sobey, I. J. (1980). On flow through furrowed channels. Part I, Calculated flow patterns. *Journal of fluid Mechanics*, 96, 1–26.